Non-Intrusive Online Stator Temperature Estimation for Open-End Winding PMSM

Nick Hunter,
Department of Electrical and Electronic Engineering
The University Of Nottingham
Nottingham, UK
nick.hunter@nottingham.ac.uk

Tom Cox
Department of Electrical and Electronic Engineering
The University Of Nottingham
Nottingham, UK
thomas.cox@nottingham.ac.uk

Pericle Zanchetta
Department of Electrical and Electronic Engineering
The University Of Nottingham
Nottingham, UK
pericle.zanchetta@nottingham.ac.uk

Shafiq Ahmed Odhano
Department of Electrical and Electronic Engineering
The University Of Nottingham
Nottingham, UK
shafiq.odhano@nottingham.ac.uk

Luca Rovere
Department of Electrical and Electronic Engineering
The University Of Nottingham
Nottingham, UK
luca.rovere@nottingham.ac.uk

Abstract—**This paper proposes a new method for online identification of stator winding temperature for an open–end winding (OEW) permanent magnet synchronous motor (PMSM). The method exploits the zero sequence current (ZSC) due to the third harmonic back electromotive force (EMF) circulating in the system in order to estimate the phase resistance, which, in turn, is used to derive the winding temperature. In order to do this a proposed idea of maximum zero sequence current amplitude along with the actual ZSC amplitude and the electrical speed of the motor is used. The temperature is estimated without any additional sensors in a wide operating speed range. A single synchronous phase-locked loop (PLL) is utilised in order to obtain the required parameters. The independence of the rotor position grants the possibility for the exploitation of the proposed winding temperature estimation method in a variety of control techniques including the sensorless control to increase the robustness of the overall system.**

Keywords—Open-end winding PMSM, stator temperature estimation, phase resistance estimation, dual inverter, zero sequence current

I. INTRODUCTION

OEW PMSM drives with common DC bus voltage are gaining increasing popularity in the pursuit of a low volume high power density solutions [1] for the aerospace [2], electric/hybrid vehicles [3] and wind power applications [4]. Moreover, such an arrangement is well suited for the implementation of different power device technology such as IGBT and Silicon Carbide (SiC) [5]. However, this topology has its drawbacks. The OEW PMSM drives with common DC link suffer from the circulating ZSC due to the third harmonic back EMF [6]. In the case when a machine is designed to be a high speed, high power and low volume it tends to have a considerably low leakage inductance. The argument is that the high speed machines have less stator coil turns. Thereby, the inductance happens to be considerably low. Less wire turns also result in a lower leakage inductance. Such a low leakage inductance prevents the drive from applying any zero sequence voltage (ZSV) [7], hence, the suppression of the aforementioned ZSC becomes impossible. The unsuppressed ZSC due to the third harmonic back EMF produces additional power loss that is converted to heat. Hence, the additional monitor of the phase winding temperature should increase the robustness of the overall system. In addition, due to a low volume and a high power density such machines tend to have either an integrated or attached liquid cooling [8]. Hence, it is crucial to track the stator temperature variations in order to ensure an optimal performance and the overall robustness of the system. This commonly requires a temperature sensor to be either integrated in or attached to the machine. This paper proposes a new non-invasive method of identification of the online stator temperature without the usage of a temperature sensor. The temperature is estimated using an estimation of the stator phase resistance. There are resistance estimation methods which have been proposed in [9] [10] involving high frequency injection, however, they tend to have an estimation error directly proportional to the rotor electrical speed, thereby, they are not suitable for the high electrical speed machines. Another method proposed recently in [11] depends on a very accurate zero crossing detection and is rather hard to implement. A rather recent paper on real-time resistance estimation requires a construction of a special function according to multiple simulations. In addition, the resistance estimation requires the direct axis voltage. [12]

A thorough analysis revealed that the information about the phase resistance is hidden inside the amplitude of ZSC caused by the third harmonic back EMF. The analysis showed that this information can be derived using a maximum zero sequence current concept introduced in this paper, the actual value of ZSC amplitude and the rotor electrical speed. Hence, a new method was proposed which utilises the ZSC due to the third harmonic back EMF freely flowing in the system in order to extract the information on the phase resistance and, thereby, estimate the online stator temperature of the system. In addition, the freely flowing ZSC due to the third harmonic back EMF in an OEW PMSM with common DC link is a convenient opportunity for utilisation of the benefits of either a sensorless control or the proposed winding temperature estimation or even both, because the temperature estimation method proposed in this paper could also potentially be combined with, for example, a novel zero-sequence model-based sensorless control [13] and could be used to compensate the rotor position estimation in any other sensorless techniques which heavily depend on the winding resistance value. Furthermore, the proposed new temperature estimation method gives an intimate temperature prediction comparing to the reading from an added temperature sensor, because the temperature sensor can only be attached to the winding insulation rather than to the winding itself. Moreover, the method could be especially beneficial for the high power low volume high speed OEW PMSM drives with common DC bus due to their problems with suppression of the ZSC, described above.
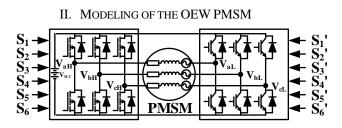
II. MODELING OF THE OEW PMSM

Fig. 1 – OEW PMSM with common DC bus

The diagram of an OEW PMSM drive with common DC link is presented in Fig. 1. The stator voltage equation, represented in machine variables:

$$V_{abc} = r_s i_{abc} + p\lambda_{abc} \qquad (1)$$

where, r_s – stator winding resistance diagonal matrix, i_{abc} – stator phase currents vector, λ_{abc} – stator phase flux linkage matrix and p is a derivative with respect to time $\left(\frac{d}{dt}\right)$ operator:

$$r_s = \begin{bmatrix} r_s & 0 & 0 \\ 0 & r_s & 0 \\ 0 & 0 & r_s \end{bmatrix}; \ V_{abc} = \begin{bmatrix} V_a \\ V_b \\ V_c \end{bmatrix};$$

$$i_{abc} = \begin{bmatrix} i_a \\ i_b \\ i_c \end{bmatrix}; \ \lambda_{abc} = \begin{bmatrix} \lambda_a \\ \lambda_b \\ \lambda_c \end{bmatrix}; \qquad (2)$$

The stator phase flux linkage λ_{abc}, in turn, is related to the stator currents i_{abc} and the rotor fundamental $\lambda_{abc(r1)}$ and the third harmonic $\lambda_{abc(r3)}$ permanent magnet flux through the following equation:

$$\lambda_{abc} = L_s i_{abc} + \lambda_{abc(r1)} + \lambda_{abc(r3)} \qquad (3)$$

where, L_s is a 3×3 inductance matrix [14], $\lambda_{abc(r1)}$ and $\lambda_{abc(r3)}$ are denoted as shown in the set of equations (4).

$$L_s = \begin{bmatrix} L_{aa} & L_{ab} & L_{ac} \\ L_{ba} & L_{bb} & L_{bc} \\ L_{ca} & L_{cb} & L_{cc} \end{bmatrix}$$

$$\lambda_{abc(r1)} = \lambda_{pm} \begin{bmatrix} \sin(\theta_e) \\ \sin\left(\theta_e - \frac{2}{3}\pi\right) \\ \sin\left(\theta_e + \frac{2}{3}\pi\right) \end{bmatrix} \qquad (4)$$

$$\lambda_{abc(r3)} = \lambda_{pm} K_{pm3} \begin{bmatrix} \sin(3\theta_e) \\ \sin\left(3\left(\theta_e - \frac{2}{3}\pi\right)\right) \\ \sin\left(3\left(\theta_e + \frac{2}{3}\pi\right)\right) \end{bmatrix}$$

where, λ_{pm} is the amplitude of flux linkage established by the permanent magnet and K_{pm3} is one third of the ratio of the amplitude of the open circuit 3rd harmonic back EMF and fundamental back EMF, respectively, induced in either of the stator windings. θ_e is the electrical rotor position. However, converting (1) to rotor ($qd0$) reference frame, where the d-axis is aligned with the north pole of the permanent magnets, a set of the PMSM voltage equations can be written as (5).

$$\begin{cases} V_q = r_s i_q + L_q \dfrac{di_q}{dt} + \omega_e L_d i_d + \omega_e \lambda_{pm} \\[2mm] V_d = r_s i_d + L_d \dfrac{di_d}{dt} - \omega_e L_q i_q \\[2mm] V_0 = r_s i_0 + L_0 \dfrac{di_0}{dt} + 3\omega_e \lambda_{pm} K_{pm3} \cos(3\theta_e) \end{cases} \qquad (5)$$

where the bottom equation is the ZSV (V_0) equation with L_0 being the leakage inductance, i_0 is the ZSC and ω_e is the electrical rotor speed.

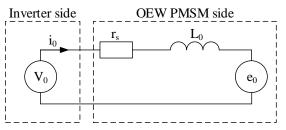## III. ZERO SEQUENCE CURRENT ANALYSIS

Fig. 2 – Equivalent circuit of zero sequence component of OEW PMSM

An equivalent circuit of the zero sequence component of equation (5) is shown in Fig. 2 – Equivalent circuit of zero sequence component of OEW PMSM. It can be seen that there are two causes of the ZSC: the third harmonic back EMF e_0 and the ZSV from the inverter side V_0. This V_0 could be used to oppose e_0, thereby, suppressing the ZSC. However, in some cases when the DC bus voltage is large and the zero sequence inductance L_0 is small the suppression of the ZSC by the means of the inverter's ZSV is not possible because introducing a modulated V_0 signal equal to a large DC bus value would result in a spike of i_0 as the value of L_0 is considerably low. In such a case it is more appropriate to let the i_0 due to e_0 to flow freely. Hence, V_0 is left 0V.

The steady state phasor form of ZSV equation (5) can be written as follows.

$$\tilde{V}_0 = r_s \tilde{I}_0 + jX_0 \tilde{I}_0 + \tilde{E}_0 \qquad (6)$$

where, $\tilde{V}_0$ and $\tilde{I}_0$ are the zero sequence voltage and current phasors, respectively, r_s is the phase resistance, X_0 is the zero sequence inductive reactance, $\tilde{E}_0$ is the zero sequence back EMF phasor with a zero phase shift and the amplitude denoted as:

$$\left|\tilde{E}_0\right| = 3\omega_e \lambda_{pm} K_{pm3} \qquad X_0 = 3\omega_e L_0 \qquad (7)$$

Simplifying equation (6) by setting V_0 to zero and substituting (7) into (6), rearranging the outcome in order to obtain the ZSC amplitude $\left|\tilde{I}_0\right|$:

$$\left|\tilde{I}_0\right| = \frac{3\omega_e \lambda_{pm} K_{pm3}}{\sqrt{r_s^2 + (3\omega_e L_0)^2}} \qquad (8)$$

Introducing a concept of the maximum possible value that ZSC amplitude can achieve by taking the limit of (8) when the electrical rotor speed ω_e tends to infinity:

$$\left|\tilde{I}_0\right|_{max} = \lim_{\omega_e \to \infty} \left(\left|\tilde{I}_0\right|\right)$$
$$= \lim_{\omega_e \to \infty} \left(\frac{3\omega_e \lambda_{pm} K_{pm3}}{\sqrt{r_s^2 + 9\omega_e^2 L_0^2}}\right) = \frac{\lambda_{pm} K_{pm3}}{L_0} \qquad (9)$$

The maximum value of $\left|\tilde{I}_0\right|$ is a good indicator for the OEW PMSM that even if the rotor will experience an

infinitely large change in position the ZSC will not exceed a certain maximum finite value. Moreover, substituting the concept of a maximum zero-sequence current of equation (9) into (8) the ZSC amplitude $|\tilde{I}_0|$ can now be written in terms of the maximum value $|\tilde{I}_0|_{max}$ and the electrical rotor speed ω_e:

$$|\tilde{I}_0| = |\tilde{I}_0|_{max} \frac{\omega_e}{\sqrt{\sigma_0{}^2 + \omega_e{}^2}} \tag{10}$$

where, σ_0 is a frequency constant that can be found using equation (11).

$$\sigma_0 = \frac{r_s}{3L_0} \tag{11}$$

Fig. 3 shows the graph of equation (10) along a range of frequencies. It was noted that the multiples of the frequency constant from equation (11) correspond to the particular percentage values of the zero-sequence current amplitude with respect to the introduced in this paper concept of the maximum ZSC amplitude.
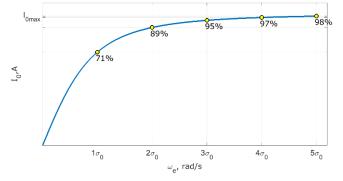

Fig. 3 – Relationship between the ZSC amplitude and the rotor electrical speed

In order to determine a frequency that corresponds to a particular ZSC amplitude the frequency constant σ_0 must be multiplied by a frequency constant multiplier n:

$$\omega_e = n\sigma_0 \tag{12}$$

The frequency constant multiplier n, in turn, can be found using the ZSC amplitude $|\tilde{I}_0|$ and the maximum ZSC amplitude value $|\tilde{I}_0|_{max}$:

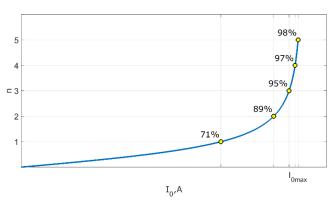$$n = \frac{|\tilde{I}_0|}{\sqrt{|\tilde{I}_0|_{max}{}^2 - |\tilde{I}_0|^2}} \tag{13}$$

Fig. 4 – Relationship between the frequency constant multiplier and the ZSC amplitude

The curve, derived from equation (13) is shown in Fig. 4. It can be observed that the frequency constant multiplier n corresponds to a particular percentage of the maximum ZSC.

IV. RESISTANCE AND TEMPERATURE ESTIMATION

A. Resistance Estimation

The amplitude of ZSC along with the electrical rotor speed contains the information about the phase resistance value through the frequency constant σ_0. Substituting equation (11) into (12) in order to obtain the phase resistance value:

$$r_s = 3L_0 \frac{\omega_e}{n} \tag{14}$$

According to equation (13), n is obtained using the maximum value of ZSC amplitude and the actual ZSC amplitude only which can be accurately estimated using a simple synchronous PLL algorithm.

B. Temperature Estimation

The stator winding temperature estimation technique employs the fact that the resistivity of a metal is affected by the temperature. Whenever the temperature of the metal is raised the free moving electrons inside the metal are colliding much more frequently. Hence, the drift velocity of the electrons caused by the electric current is much less because they have to go against all of the random collisions that are occurring inside the metal. As a result, the temperature raise increases the metals resistivity according to the equation (15) below. [15]

$$\rho_T = \rho_0[1 + \alpha(T - T_0)] \tag{15}$$

Where, ρ_T is the metal resistivity at temperature T, ρ_0 is the resistivity at the reference temperature T_0 and α is the temperature coefficient of resistivity. The relationship between the temperature T and resistivity ρ allows to exploit the phase resistance R to determine the winding temperature assuming that the length of the wire L and the cross sectional area A remain the same, hence $L_T = L_0$ and $A_T = A_0$, respectively.

$$R = \rho \frac{L}{A} \quad \Rightarrow \quad \frac{R_T}{R_0} = \frac{\rho_T \frac{L_T}{A_T}}{\rho_0 \frac{L_0}{A_0}} \quad \Rightarrow \quad \frac{R_T}{R_0} = \frac{\rho_T}{\rho_0} \tag{16}$$

Therefore, substituting (16) into (15):

$$R_T = R_0[1 + \alpha(T - T_0)] \tag{17}$$

$$T = \frac{1}{\alpha}\left(\frac{R_T}{R_0} - 1\right) + T_0 \tag{18}$$

Where, R_T is the copper resistance at temperature T, R_0 is the resistance at the reference temperature T_0 and α is the temperature coefficient of copper resistivity. According to the standard values of temperature coefficient of annealed copper $\alpha = 0.0394/°C$ [16]. Using the derived equation of the temperature (18) and the estimated phase resistance R_T along with the temperature coefficient α and the measured beforehand phase resistance R_0 at the reference temperature T_0, the current winding temperature T can be estimated.

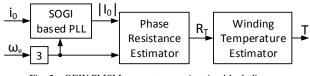## C. Implementation of Resistance and Temperature Estimation

Fig. 5 – OEW PMSM temperature estimation block diagram

Fig. 5 represents a combination of the resistance estimation technique derived in equation (14) and the temperature estimation in equation (17).

The process of derivation of i_0 is rather simple and does not involve the rotor position:

$$i_0 = \frac{i_a + i_b + i_c}{3} \tag{19}$$

The amplitude of the zero sequence current is provided by the modified version of the second order generalised integrator (SOGI) based single phase Phase-Locked-Loop (PLL) (Fig. 5, Fig. 6, and Fig. 8) and explained in [17]. The modification added is the amplitude identification bit at the output of the mentioned PLL, as illustrated in Fig. 6.
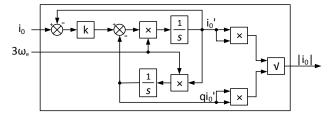

Fig. 6 – SOGI based single phase PLL amplitude estimator

The direct $i_0{'}$ and the quadrature $qi_0{'}$ output signals are used in the following formula to calculate the ZSC amplitude $|i_0|$ for the current limiter.

$$|i_0| = \sqrt{(i_0{'})^2 + (qi_0{'})^2} \tag{20}$$

The ZSC's amplitude is also used in the current reference limiter, shown in Fig. 8. This special current limiter takes into consideration the direct current and the amplitude of the ZSC in order to provide the machine with the maximum allowed RMS current. The RMS value of a signal is a square root of the squares of all of the harmonics RMS values that comprise the signal itself. The phase current of the considered OEW PMSM consists of the fundamental and the zero sequence currents mainly. Hence, the following equation appears to be an appropriate limit for the phase current:

$$I_{RMS\_lim} = \sqrt{\left(\frac{\sqrt{i_{q\_lim}{}^2 + i_d{}^2}}{\sqrt{2}}\right)^2 + \left(\frac{|i_0|}{\sqrt{2}}\right)^2} \tag{21}$$

where, I_{RMS_lim} is the RMS current limit, i_{q_lim} is a particular limit for the quadrature current, i_d is the direct current, and $|i_0|$ is the amplitude of the zero-sequence current. Solving the equation (21) for i_{q_lim}:

$$i_{q\_lim} = \sqrt{2I_{RMS\_lim}{}^2 - i_d{}^2 - |i_0|^2} \tag{22}$$

The new limit for the quadrature axis current can be implemented according to (22).

As it was already mentioned, the zero-sequence voltage for the machines under consideration in this paper is not allowed. In order to ensure that there is no ZSV produced by the modulation, a special space vector voltage modulation (SVM) technique is used. Such a modulation technique eliminates the ZSV produced by the voltage source converter (VSC). This is realised using only certain voltage vectors that do not produce ZSV. The particular voltage vectors are depicted in Fig. 7 in red. Thereby, according to Fig. 7, the voltage limit for the VSC appears to be V_{DC} (magenta circle). This technique is explained in [5].
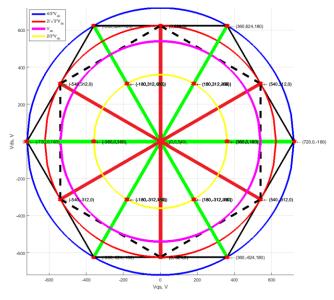

Fig. 7 – SVM diagram for the dual fed inverter

The simulation illustrated in Fig. 8 features the aforementioned special modulation technique that is used in order to keep the ZSV always zero. The simulation clock frequency was set to be the same as the carrier counter of the actual modulator, 100MHz. Hence, the simulation very accurately imitates the behaviour of an FPGA based modulator.

The sampling frequency of the controller was set to be 40 kHz to represent the actual switching frequency of a SiC inverter.

The variable parameters that are needed from the proposed method are the amplitude of ZSC and the electrical rotor speed. This information can be obtained with a virtually zero steady state estimation error by introducing the SOGI based PLL that has already been discussed above.

D. Parameter Sensitivity Analysis

The estimation of both the resistance and, subsequently, the temperature rely on the third harmonic flux ($\lambda_{pm}K_{pm3}$) parameter and the zero-sequence inductance (L_0) parameter. These parameters are considered to have insignificant variations with the motors allowed operating temperature. This makes the proposed method more robust. Nonetheless, the produced parameter sensitivity analysis is based upon an assumption that the third harmonic flux ($\lambda_{pm3} = \lambda_{pm}K_{pm3}$) could vary by 5% and the zero-sequence inductance (L_0) could vary by 10%. However, the variation of the maximum zero-sequence current due to the third harmonic back EMF,

$\left|\tilde{I}_0\right|_{max}$, which, according to the equation (11), represents the ratio $\frac{\lambda_{pm}K_{pm3}}{L_0}$ can in such a case vary from -13% to +16.7%.
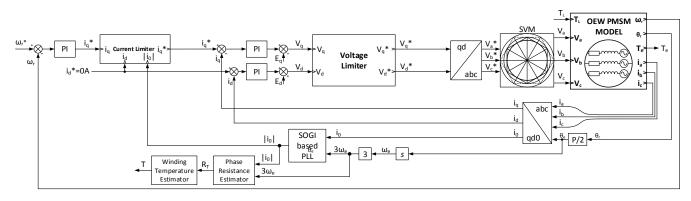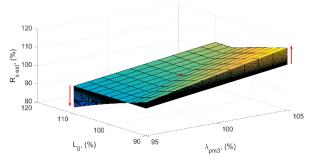

Fig. 8 – Simulation block diagram

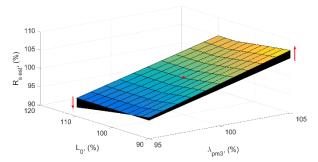Fig. 9 – Resistance estimation parameter sensitivity with increasing electrical speed from 10 to 800 Hz at T = 20°C
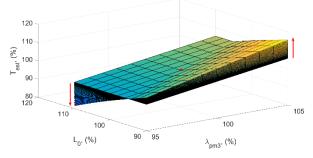

Fig. 11 – Temperature estimation parameter sensitivity with increasing electrical speed from 10 to 800 Hz at T = 45°C

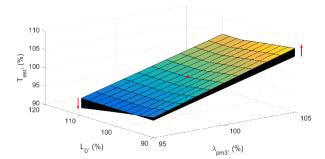Fig. 10 – Resistance estimation parameter sensitivity with increasing electrical speed from 10 to 800 Hz at T = 100°C

Fig. 12 – Temperature estimation parameter sensitivity with increasing electrical speed from 10 to 800 Hz at T = 100°C

The parameter sensitivity analysis is shown in Fig. 9 - Fig. 12. The electrical speed was raised from 10 to 800 Hz. The red dot in the middle represent the correct parameter identification at the correct values of the parameters in consideration. The direction of the red arrows signify the direction of the error growth with increasing speed. The error ranges according to Fig. 9 to Fig. 12 were recorded in TABLE II.

TABLE I ESTIMATION ERROR WITH $L_0 = \pm5\%$ AND $\lambda_{pm3} = \pm10\%$

Actual Temperature °C	Error range with increasing speed 10 to 800 Hz	
	Estimated Resistance, %	Estimated Temperature, %
45	-17 - +14	-19 - +116
100	-8 - +8	-8 - +8

However, the higher value of temperature tend to depend less on frequency.

V. SIMULATION RESULTS

The proposed winding temperature estimation method was tested in Matlab/Simulink using a machine the parameters of which are listed in TABLE II.

TABLE II 3-PHASE OEW PMSM SPECIFICATION

Parameter	Value
Rated Speed, $\omega_{r\ rated}$	20kRPM
Phase Resistance, R_s	164mΩ
q-axis Inductance, L_q	355µH
d-axis Inductance, L_d	355µH
Leakage Inductance, L_0	17.75µH
PM Flux Linkage, λ_{pm}	71.5mVs
3rd Harmonic Flux Linkage coefficient, K_{pm3}	0.0115
Poles, P	6
Rated Current, I_{max}	150A
Rated Voltage, V_{DC}	540V

Considerably low leakage inductance prevents the suppression of ZSC in such a machine as an introduction of a

540V DC ZSV even for a short duration can result in a large ZSC spike. For example, the drive described in Table I produces a 30A current spike if the ZSV equal to the DC bus voltage is applied even for as little as one microsecond. Hence, an obvious option for such types of drives would be to allow ZSC due to the third harmonic back EMF to flow freely in the system and ensure that there are no ZSV applied by the inverter. Although this would cause an additional loss, it creates an opportunity for estimation of the stator winding temperature.

During the simulation time, the PMSM speed was set to be of a constant value: 100 Hz and 800Hz electrical for two cases. Different load torque steps were applied: 1, 10, 20, 30, and 40 Nm every second, respectively. The reference temperature was increased exponentially from 20 to 100°C. The simulation results are shown in Fig. 13. The simulation has shown that the estimated values of temperature and resistance tracks the actual values of the same parameters with an insignificant error in both cases: for 100Hz and 800Hz electrical speed.
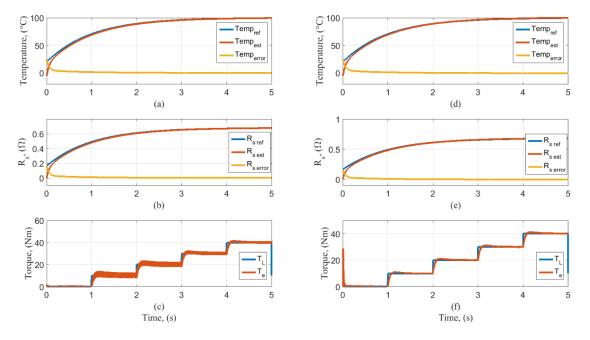

Fig. 13 – Simulation results: (a,b,c) – 800Hz constant electrical speed, (d,e,f) – 100Hz constant electrical speed

VI. CONCLUSIONS

The third harmonic of the back EMF causes the zero sequence currents to circulate in the OEW PMSM drives with common DC bus. In case of a low leakage inductance it is impossible to suppress ZSC due to the third harmonic back EMF. Hence, this current is left flowing in the system. The new online temperature estimation method proposed in this paper and validated through simulation benefits from the mentioned ZSC by using it to derive the information about the stator temperature. Thereby, it offers an alternative solution for the temperature monitoring of the OEW PMSM drives with common DC link. The proposed method relies on the variable parameters such as the amplitude of ZSC and the rotor speed that can be estimated with virtually zero estimation error at steady state. Hence, the method could also be suitable for the sensorless control. The proposed method will be especially beneficial for a particular type of machines such as the one used in order to validate the proposed idea in simulation. The power density of that machine is achieved relying on an internal liquid cooling. Hence, the proposed method of the temperature estimation can improve the robustness of the overall system by introducing the system's protection mechanisms based on the stator temperature monitoring. It is especially beneficial when the ZSC is left flowing freely in the motor winding as it creates an additional power loss into heat that now can be monitored. There is no need for a position sensor to be able to use the method, hence, the system's reliability can further be increased. The possibility of implementation of the proposed method together with a variety of different control techniques for OEW PMSM including the sensorless control such as that described in [13] is also one of the advantages. The proposed method works with any common DC bus voltage OEW PMSM control technique that does not introduce the ZSV from the inverter side. The estimation is run without interrupting the control process. The proposed new method involving the phase resistance estimator is also beneficial for online self-tuning of those controllers which are heavily dependent on the stator resistance value.

REFERENCES

[1]   P. Zanchetta, C. Gerada, A. Lidozzi, M. Degano, F. Crescimbini and L. Solero, "Performance evaluation of converter topologies for high speed Starter/Generator in aircraft applications," in *40th Annual Conference of the IEEE Industrial Electronics Society*, Dallas, TX, 2014.

[2]   S. Mohan, J. S. T.K, A. Gopinath, J. B and M. Namboothiripad, "Modeling and simulation of high power open end winding based electromechanical actuator for aerospace applications," in *International Conference on Power and Advanced Control Engineering (ICPACE), 2015*, Bangalore, India, 2015.

[3]   B. Lin, D. Sun and Y. Chen, "Research on high-speed operation of hybrid-inverter fed open winding

permanent magnet synchronous motor," in *International Conference on Electrical Machines and Systems (ICEMS), 2013*, Busan, South Korea, 2014.

[4] H. Zhan, Z. Q. Zhu and M. Odavic, "Nonparametric Sensorless Drive Method for Open-Winding PMSM Based on Zero-Sequence Back EMF With Circulating Current Suppression," *IEEE Transactions on Power Electronics,* vol. 32, no. 5, pp. 3808 - 3817, 2017.

[5] L. Rovere, A. Formentini, G. L. Calzo, P. Zanchetta and T. Cox, "IGBT-SiC dual fed open end winding PMSM drive," in *Electric Machines and Drives Conference (IEMDC), 2017 IEEE International*, Miami, 2017.

[6] P. Sandulescu, F. Meinguet, X. Kestelyn, E. Semail and A. Bruyere, "Control Strategies for Open-End Winding Drives Operating in the Flux-Weakening Region," *IEEE Transactions on Power Electronics,* vol. 29, no. 9, pp. 4829 - 4842, 2014.

[7] Q. An, J. Liu, Z. Peng, L. Sun and L. Sun, "Dual-Space Vector Control of Open-End Winding Permanent Magnet Synchronous Motor Drive Fed by Dual Inverter," *IEEE Transactions on Power Electronics,* vol. 31, no. 12, pp. 8329-8342, 2016.

[8] P. Arumugam, Z. Xu, A. L. Rocca, G. Vakil, M. Dickinson, E. Amankwah, T. Hamiti, S. Bozhko, C. Gerada and S. J. Pickering, "High-Speed Solid Rotor Permanent Magnet Machines: Concept and Design," *IEEE Transactions on Transportation Electrification,* vol. 2, no. 3, pp. 391 - 400, 2016.

[9] G. Feng, C. Lai, K. L. V. Iyer and N. C. Kar, "Improved High-Frequency Voltage Injection Based Permanent Magnet Temperature Estimation for PMSM Condition Monitoring for EV Applications," *IEEE Transactions on Vehicular Technology,* vol. 67, no. 1, pp. 216-225, 2018.

[10] G. Feng, C. Lai and N. C. Kar, "Expectation-Maximization Particle-Filter- and Kalman-Filter-

Based Permanent Magnet Temperature Estimation for PMSM Condition Monitoring Using High-Frequency Signal Injection," *IEEE Transactions on Industrial Informatics ,* vol. 13, no. 3, pp. 1261 - 1270, 2016.

[11] M. Pulvirenti, G. Scarcella, G. Scelba, A. Testa and M. M. Harbaugh, "On-line stator resistance and permanent magnet flux linkage identification on open-end winding PMSM drives," in *Energy Conversion Congress and Exposition (ECCE), 2017 IEEE*, Cincinnati, OH, USA, 2017.

[12] G. Kizir, Ş. Demirbaş and M. Şahin, "Real-time resistance estimation of permanent magnet synchronous motor," in *2018 IEEE 12th International Conference on Compatibility, Power Electronics and Power Engineering (CPE-POWERENG 2018)*, Doha, 2018.

[13] H. Zhan, Z. Q. Zhu, M. Odavic and Y. Li, "A Novel Zero-Sequence Model-Based Sensorless Method for Open-Winding PMSM With Common DC Bus," *IEEE Transactions on Industrial Electronics,* vol. 63, no. 11, pp. 6777 - 6789, 2016.

[14] P. Krause, O. Wasynczuk, S. Sudhoff and S. Pekarek, Analysis of Electric Machinery and Drive Systems, Hoboken: John Wiley & Sons Inc, 2013.

[15] R. H. PAUL PETER URONE, College Physics, Houston,: OpenStax, 2017.

[16] F. A. Wolff and J. H. Dellinger, "The electrical conductivity of commercial copper," *Proceedings of the American Institute of Electrical Engineers,* vol. 29, no. 12, pp. 1981-2008, 1910.

[17] M. Ciobotaru, R. Teodorescu and F. Blaabjerg, "A new single-phase PLL structure based on second order generalized integrator," in *2006 37th IEEE Power Electronics Specialists Conference*, Jeju, 2006.